Surfaces and Interfaces xxx (xxxx) 100984

Contents lists available at ScienceDirect

Surfaces and Interfaces

journal homepage: www.elsevier.com/locate/surfin

Large enhancement of photocatalytic activity in ZnO thin films grown by plasma-enhanced atomic layer deposition

Ales Omerzu[a, b, *], Robert Peter[a, b], Daria Jardas[a, b], Iztok Turel[c], Kresimir Salamon[d], Matejka Podlogar[e], Damjan Vengust[e], Ivana Jelovica Badovinac[a, b], Ivna Kavre Piltaver[a, b], Mladen Petravic[a, b]

[a] University of Rijeka, Department of Physics, R. Matejcic 2, 51 000 Rijeka, Croatia
[b] University of Rijeka, Centre for Micro- and Nanosciences and Technologies, R. Matejcic 2, 51 000 Rijeka, Croatia
[c] Faculty of Chemistry and Chemical Technology, University of Ljubljana, Vecna pot 113, 1000 Ljubljana, Slovenia
[d] Rudjer Boskovic Institute, Bijenicka cesta 54, HR-10000 Zagreb, Croatia
[e] Jozef Stefan Institute, Jamova 39, 1000 Ljubljana, Slovenia

ARTICLE INFO

Keywords:
Zinc oxide
Thin film
Atomic layer deposition
Plasma
Photocatalysis

ABSTRACT

In this work, we present a large, tenfold enhancement in the photocatalytic activity of thin ZnO films grown by plasma-enhanced atomic layer deposition (PE-ALD) at 100 °C, compared to values obtained for thin ZnO films deposited by a conventional thermal ALD method at the same temperature. Thus, we have demonstrated that we can deposit thin ZnO films using the PE-ALD method both at low temperatures and with a high photocatalytic ability. A number of structural (SEM, EDX, HRTEM, GIXRD, XRR, XPS, SIMS) and optical (UV-Vis, PL) experimental techniques have been employed to elucidate a possible physical origin of the observed remarkable difference in the photocatalytic activity of thin ZnO films grown by the PE-ALD method compared to those grown by the thermal ALD method.

1. Introduction

Zinc oxide (ZnO) has been known as a white powder polycrystalline material for centuries and has been used mainly as a white pigment. With the advent of modern electronics in the 1920s and 1930s, research on electronic properties of ZnO and its first applications in electronics as a material for rectifiers and varistors have started [1]. The electronic properties of ZnO are still extensively explored for the development of novel biosensors and gas sensors, transparent thin-film transistors (TFTs), optical devices or solar cells [2]. A systematic research on the photocatalytic properties of ZnO started in the early 1950s [3,4] and continues until today. ZnO is a wide gap semiconductor (E_g = 3.2 -3.4 eV) that can be photoexcited with UV light and thus charged with additional free charge carriers. The role of photo-excited electrons and holes in photocatalytic processes has been well established since 1967 [5], when quantitative experiments on ZnO single crystals have demonstrated that chemical processes of reduction and oxidation in aqueous solutions are initiated by photocreated electrons and holes, respectively, which could successfully migrate to the surface of a ZnO sample. The first applications of ZnO in photo-degradation of organic water pollutants have appeared in the mid-1990s [6] using ZnO in the form of fine powder. Very soon, it became evident that it would be more advantageous to fix the photoactive ZnO material on a rigid support in order to remove the photocatalyst from the solution more easily later, after the photodegradation process is completed. For this reason, extensive applications of thin ZnO films in photodegradation processes were started in the early 2000s [7].

ZnO can be synthesised in the form of a thin film by various techniques: RF magnetron sputtering [8], ion beam sputtering (IBS) [9], molecular beam epitaxy (MBE) [10,11], chemical vapour deposition (CVD) [12,13], atomic layer deposition (ALD) [14] or pulsed laser deposition (PLD) [15,16]. Each of these techniques has a different balance of characteristics that are commonly required in practice, e.g. sample quality (crystallinity), deposition rate, low cost, etc. Among them, ALD has some unique features. For example, by varying the ALD parameters (mainly deposition temperature), one can synthesise thin ZnO films with a wide range of structural (crystal grain sizes and orientations, chemical composition) and physical (electrical conductivity, optical absorption, photoluminescence) properties. An even more important specific property of the ALD method, especially for photocatal-

* Corresponding author.
E-mail address: aomerzu@uniri.hr (A. Omerzu).

https://doi.org/10.1016/j.surfin.2021.100984
Received 14 September 2020; Received in revised form 17 January 2021; Accepted 29 January 2021

ysis applications [17], is the ability to deposit conformal thin films on highly corrugated and even porous substrates [18] with nanometre-scale thickness control [19].

The ALD temperature window for the deposition of thin, stoichiometric ZnO films spans a temperature range between 120 °C and 180 °C. For many applications, such as the use of thermosensitive substrates, it is prerequisite to perform ALD deposition at lower temperatures [20]. Recently, it has been shown that thin ALD films of ZnO deposited at 100 °C and below exhibit significant photocatalytic ability [21]. However, compared to the films synthesised at temperatures above 150 °C [22], their photocatalytic activity is much weaker. To facilitate the ALD process at temperatures below the ALD temperature window, one can use the plasma enhanced atomic layer deposition (PE-ALD) process [23]. The PE-ALD process generally uses the same precursor for zinc (diethylzinc – DEZ), but plasma-activated O_2 gas is used for the oxygen precursor, instead of water [24]. Compared to thermally grown ZnO ALD films, the films grown by the PE-ALD method have a smaller grain size and a preferential (100) growth direction [24], a high electrical resistivity [25], a low charge carrier density and carrier mobility [26], a much stronger excitonic emission [27] and an atomic Zn/O ratio lower than the stoichiometric one [28,29].

The photocatalytic properties of the ZnO films grown by the PE-ALD method have not been tested so far. The aim of the present work was to investigate and explain the differences in the photocatalytic activity of thin ZnO films grown by either the PE-ALD or the regular thermal ALD method by measuring the physical properties of the two types of films using a range of structural and optical experimental techniques. Among the latter, photoluminescence is particularly closely related to photocatalytic processes, since both photoluminescence and photocatalytic properties depend on the type and concentration of defects (i.e. charge traps) in a material [30, 31, 32].

2. Materials and methods

2.1. ALD synthesis

Atomic layer deposition of ZnO thin films was carried out in Beneq TFS 200 system at a deposition temperature of 80 °C. For the PE-ALD growth, DEZ (STREM Chemicals) and O_2 gas plasma were used as zinc and oxygen precursors, respectively. The growth cycles for PE-ALD deposition included pulses of DEZ (250 ms) followed by a 1.25 s purge with N_2 gas (purity 6.0), 3 s plasma exposure and 6 s purge with high-purity nitrogen. The capacitively-coupled plasma source was operated at 13.56 MHz and 150 W. For thermal ALD growth, the pulse times for DEZ and deionized H_2O were 200 ms and 180 ms, respectively, followed by 1 s purge cycles with N_2 gas. The ALD synthesis parameters for thermal ALD and PE-ALD deposition of ZnO thin films are outlined in Table 1. Glass microscope slides (for photocatalytic activity measurements and XRD), fussed silica wafers (for optical measurements) or silicon wafers (for HRTEM, XPS, XRD, SEM, EDX and SIMS characterization) were used as substrates for bot types of films. The film thickness was monitored with SEM and it was determined to be in the range of 100 ±10 nm for all samples.

Table 1
The ALD synthesis parameters for thermal ALD and PE-ALD depositions of ZnO thin films used in further experiments.

Thermal ALD		**PE-ALD**	
pulse	*duration*	*pulse*	*duration*
DEZ	200 ms	DEZ	250 ms
purge	1 s	purge	1.25 s
H_2O	180 s	O_2 plasma (150 W)	3 s
purge	1 s	purge	6 s

2.2. Characterisation of morphology, crystal structure and chemical composition

Surface morphology was examined using a Jeol JSM-7800F SEM instrument (Jeol Ltd., Tokyo, Japan) with an electron beam accelerating voltage of 10 kV and a working distance (WD) of 2 mm. The EDX analysis was performed on the same instrument with an electron beam accelerating voltage of 12 kV. A more detailed structural information on grain size and orientation was obtained using the conventional TEM operating at 200 kV (JEM 2100, Jeol Ltd., Tokyo, Japan). Fast Fourier transform (FFT) and other image analyses were performed using Gatan Micrograph software.

The crystal structure of the samples was studied by grazing incidence X-ray diffraction (GIXRD) method. The GIXRD measurements were performed on a diffractometer equipped with a Co X-ray tube and a W/C multilayer for beam shaping and monochromatization. Diffracted spectra were collected with a curved position sensitive detector (RADICON) placed 120 mm from the sample. The GIXRD measurements were performed at a fixed grazing incidence angle of $\alpha_i = 1°$, where the X-ray penetration depth covers the thickness of the ZnO films. X-ray reflectivity (XRR) was used to determine thickness and average density of the ZnO films. The XRR measurements were performed using the same setup as the GIXRD, but with a different detector (Hecus PSD-50M) located 500 mm from the sample. The XRR data were collected using a series of diffuse scattering spectra as a function of incidence angle α_i ($0° < \alpha_i < 2.5°$, step 0.003°) from which the intensity of specular refection, corrected for background and diffuse component, was determined.

X-ray Photoelectron Spectroscopy (XPS) measurements were performed in a SPECS spectrometer equipped with a monochromatized source of Al Kα X-rays of 1486.74 eV and the Phoibos MCD 100 electron energy analyzer. The typical pressure in the UHV chamber was in the range of 10^{-7} Pa. The photoemission spectra around the Zn $2p_{3/2}$ and the O 1*s* core levels were recorded with the electron pass energy of 10 eV. The experimetal XPS curves were deconvoluted using several sets of mixed Gaussian–Lorentzian functions with Shirley background subtraction [33].

The Hiden SIMS instrument, equipped with the quadrupole mass analyzer, was used for secondary ion mass spectrometry (SIMS) measurements, collecting positive Zn and O ions during sputtering with 3 keV Ar^+ primary ions at an incident angle of 45°.

2.3. Optical spectroscopy

For optical spectroscopy measurements, we used 100 nm thick ZnO films deposited on UV-grade fused silica substrates. The optical absorption was measured with the Perkin Elmer Lambda 750 UV-Vis-NIR spectrophotometer in the spectral range from 200 nm to 800 nm. The photoluminescence emission and excitation spectra were measured on the same samples using Perkin Elmer LS 55 fluorimeter in the same spectral range.

2.4. Photocatalytic activity testing

The photocatalytic activity of the thin films was tested by monitoring the decomposition of methylene blue (MB) in deionized water under UV illumination. The solution had the initial MB concentration of 4×10^{-5} M, the volume of 15 mL, while the active surface of the thin ZnO films had the lateral dimensions of 1 cm x 3 cm. The solutions were illuminated with the Osram UV lamp HNS 6 W G5. A decay of MB concentration was measured by recording the optical absorption of MB at 664 nm at constant time intervals of 60 min.

3. Results and discussion

3.1. Structure and chemical composition

The surface morphologies, as obtained by SEM, for the films synthesised by the ALD and the PE-ALD methods are shown in Fig. 1. The ALD film (Fig. 1 a)) consists of densely packed well-defined grains with sizes between 10 nm and 20 nm. Compared to the ALD film, the PE-ALD film (Fig. 1 b)) consists of much smaller grains (5 nm to 10 nm).

A detailed TEM study reveals more information about the grain crystallinity and morphology of both films. High-magnification images of the samples (Fig. 2 a) and b)) confirm the grain size distribution already estimated from SEM images. For the PE-ALD sample (Fig. 2 b), the grains are more clearly visible than in the SEM image. Their size range from 5 nm to 10 nm and they appear rounded. FFT (Fig. 2 d) of the high resolution (HR) image shows a clearly visible diffraction pattern corresponding to the (010) and (011) planes of wurtzite-type ZnO. The (002) diffraction spots are barely resolvable, presumably because the crystals are small and the intensity of the (002) diffraction peak is the smallest among the three. For the ALD sample, a high magnification TEM image (Fig. 2 a) reveals that the grains are columnar (extended along the surface normal direction), with some of them grown throughout the entire thickness of the film. In the lower region, they appear smaller, while in the upper region of the film they become ticker and have diameters up to 25 nm. The high magnification image shows that the single grain retains its crystallinity, but the bright and dark contrast in the HR image along the growth direction indicates that the structure is likely to consists of stacking faults and other two-dimensional defects. Similar to the PE-ALD film, the (010) and (011) diffraction spots are clearly visible in the FFT image, but this time the diffraction spots corresponding to the (002) planes are also resolvable. Most of the later planes are oriented in the direction of growth, as can be seen in Fig. 2 c (indicated by a single arrow). Similar to hydrothermally grown films, [34] pointed grains usually grow all the way to the top but exhibit reduced dimensionality due to structural defects, which is expressed as bright lines in the Fourier diffraction pattern along the growth direction (Fig. 2 c, indicated by a double arrow).

Similar observation about structural differences between the two films can also be inferred from the GIXRD spectra (Fig. 3). For both, the ALD and PE-ALD films, the position of the GIXRD peaks in the experimental curves coincides eith the diffraction peaks of the wurtzite ZnO powder, indicated at the bottom of Fig. 3. However, the relative intensities of the measured Bragg peaks show that the ZnO crystallites are preferentially orientated. The spectrum of the ALD film shows the dominant (002) peak, which means that the c-axis of most ZnO crystallites is oriented within +/-15° to the normal of the film surface [35]. On the other hand, the strongest (100) peak for the PE-ALD film is consistent with the (100) type of texture, although the texture is much less pronounced. In other words, the fraction of randomly oriented ZnO crystallites is larger in PE-ALD films than in thermal ALD films.

XRR measurements have shown that the density of the PE-ALD film, determined from the critical angle [36], is ~ 20% lower than the bulk density of ZnO, while no density deficiency was found for the ZnO film deposited by the thermal ALD method.

Further information on the chemical composition was obtained from the XPS measurements. The photoemission around O 1*s* core-levels (Fig. 4 b) implies a large deviation in the chemical composition of the PE-ALD film. While the Zn $2p_{3/2}$ spectra show a symmetrical structure with peaks from both ALD and PE-ALD surfaces centred at the binding energy (BE) of 1022.4 eV, characteristic of Zn^{2+} ions in ZnO. The O 1s spectra consist of two components: the main peak at BE of 531.5 eV (attributed to photoemission from O^{2-} ions in a ZnO matrix)

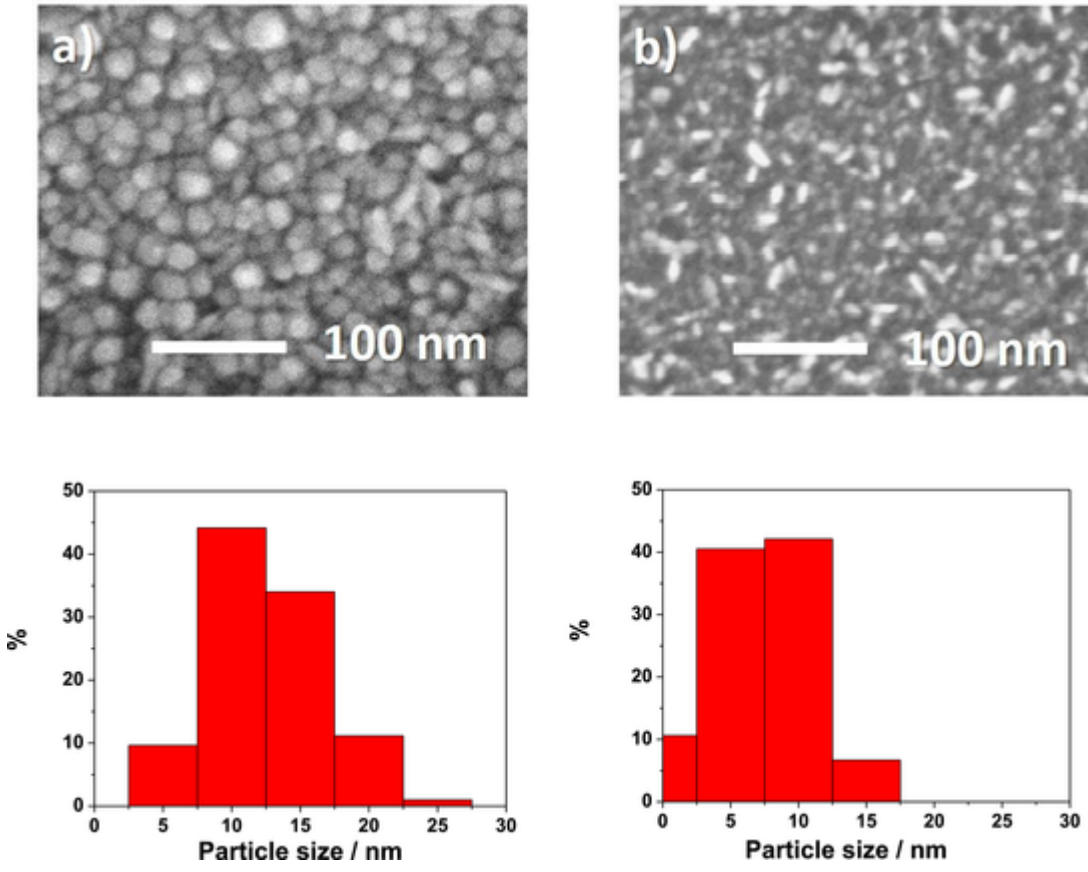

Fig. 1. SEM images of the topographies of ALD, (a) and PE-ALD, (b) thin ZnO films. The histograms below each image show the crystal size distribution obtained using ImageJ software.

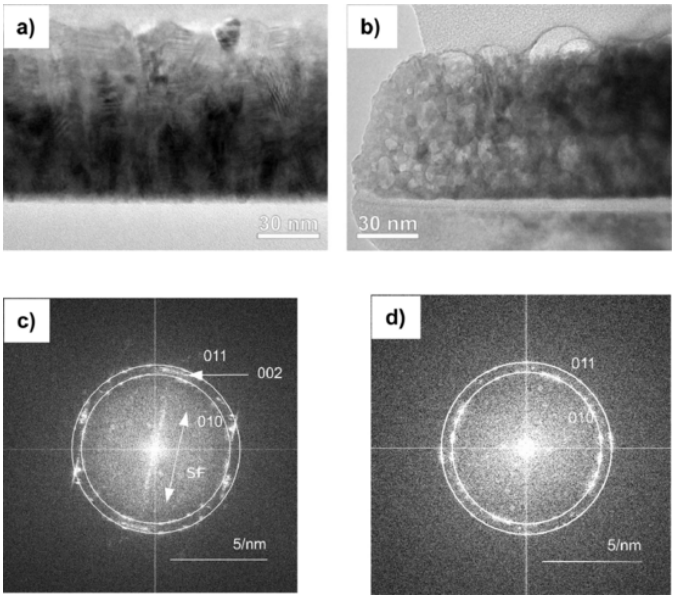

Fig. 2. HRTEM images of thin film cross sections for ALD, (a) and PE-ALD, (b) thin ZnO films. FFT of HRTEM images for ALD, (c) and PE-ALD, (d) thin ZnO films.

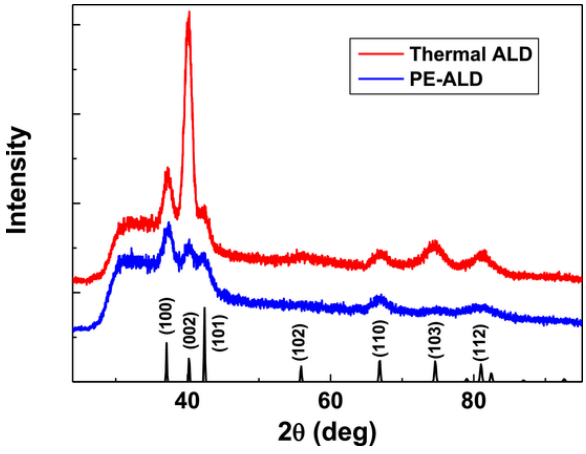

Fig. 3. GIXRD spectra of ALD and PE-ALD thin ZnO films.

and a smaller peak shifted to the higher BE (533.0 eV). The smaller peak is usually attributed to oxygen contamination by O-H groups from the surface [37, 38]. However, low coordinated oxygen ions, i.e. the oxygen ions adjacent to the Zn vacancies, have also been identified as responsible sites for the photoemission at 533 .0 eV [39, 40]. Therefore, a higher intensity of the 533.0 eV peak in the PE-ALD sample may indicate a deficiency of Zn atoms (Zn vacancies) in this sample.

XPS measurements also allow the determination of the Zn/O atomic ratio from the integrated areas under the fitting curves of the experimental Zn $2p_{3/2}$ and O 1*s* peaks (after Shirley background subtraction), normalized to the corresponding values obtained from a stoichiometric epitaxial ZnO thin film. In this way, the Zn/O atomic ratio of 0.85 was found for the plasma-deposited film, while the expected, nearly stoichiometric value was obtained for the thermally grown ZnO film, which is in agreement with the results in [41].

Further evidence for the nonstoichiometric composition of the PE-ALD film was provided by SIMS measurements on both films (see Supplementary Material). Indeed, the relative SIMS intensities of the Zn and O profiles measured on ALD and PE-ALD films show the same 15% Zn atomic deficiency in the PE-ALD film. EDX analysis has shown (see Supplementary Material) that the atomic ratio of Zn is 16 % lower in

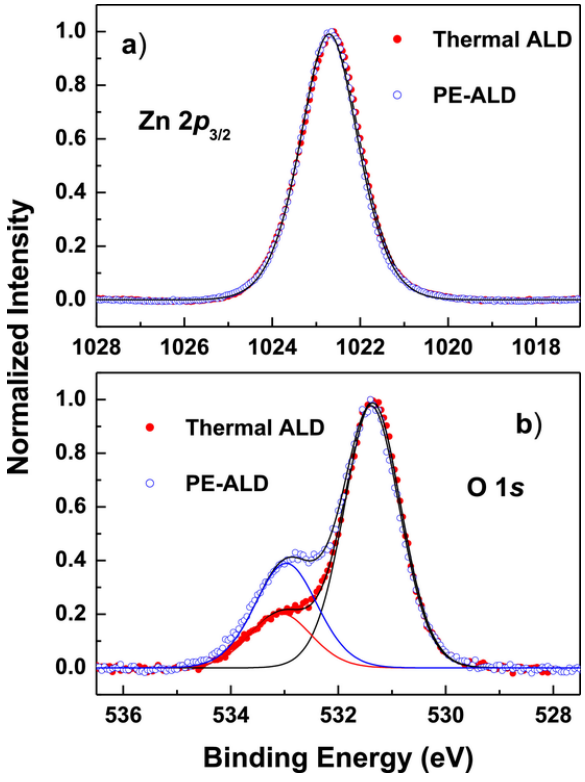

Fig. 4. XPS photoemission spectra of PE-ALD and ALD grown ZnO thin films recorded around (a) Zn $2p_{3/2}$ and (b) O 1*s* core-levels. The experimental curves are represented by open circles, while the solid lines represent numerical fits.

the PE-ALD sample, which agrees almost exactly with the values obtained by the XPS and SIMS methods.

However, the Zn deficiency is not high enough to explain the 20% lower density of the PE-ALD films (as found with XRR), where every fourth Zn atom should be missing in the crystal structure. Therefore, we suggest that about half of the density decrease could be attributed to the porosity of the PE-ALD film, although this cannot be clearly confirmed by the HRTEM image (Fig. 2 b).

3.2. Optical absorption and photoluminescence

The optical properties of the PE-ALD thin ZnO film also differ significantly from those of the ZnO ALD film. The optical absorption is much more smeared below 400 nm (Fig. 5 a), indicating a less ordered crystal structure, while the semiconductor bandgap of $E_g^{PEALD} = 3.52$ eV is strongly blue-shifted to compared to the value for the ALD thin film $E_g^{ALD} = 3.26$ eV (both determined from a Tauc plot shown in Fig. 5 b).

Photoluminescence (PL) measurements have shown even larger differences between PE-ALD and ALD samples. The intensity of excitonic band-to-band photoemission, centered at 390 nm, is greatly enhanced in the PE-ALD film (Fig. 6 a), as photoexcitation is much more efficient in both the UVC (280 nm to 315 nm) and UVB (200 nm to 280 nm) spectral regions (Fig. 6 b).

A similar difference in PL between thermally and PE-ALD grown ZnO thin films has already been observed by others [27]. That the intensity of UV excitonic emission depends on the stoichiometry of a ZnO film has been found previously in experiments on thin ZnO films synthesized by the magnetron sputtering method [42]. Namely, the intensity of excitonic emission is generally higher in films with higher oxygen content.

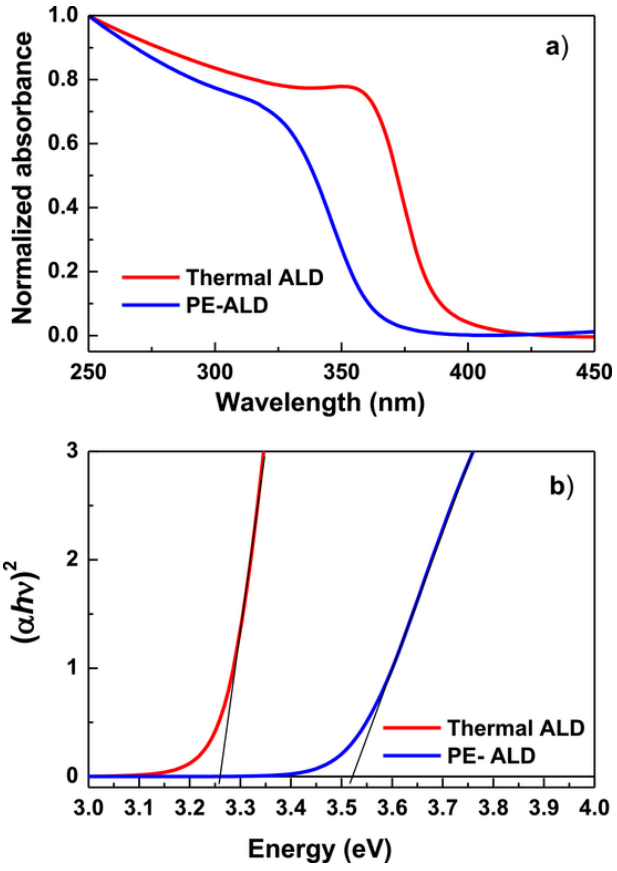

Fig. 5. Optical absorption spectra of ALD and PE-ALD thin ZnO films (a), and the same spectra plotted in a Tauc plot (b) from which the semiconductor band gaps were determined: E_g (ZnO – ALD)) = 3.26 eV and E_g (ZnO – PE-ALD)) = 3.52 eV.

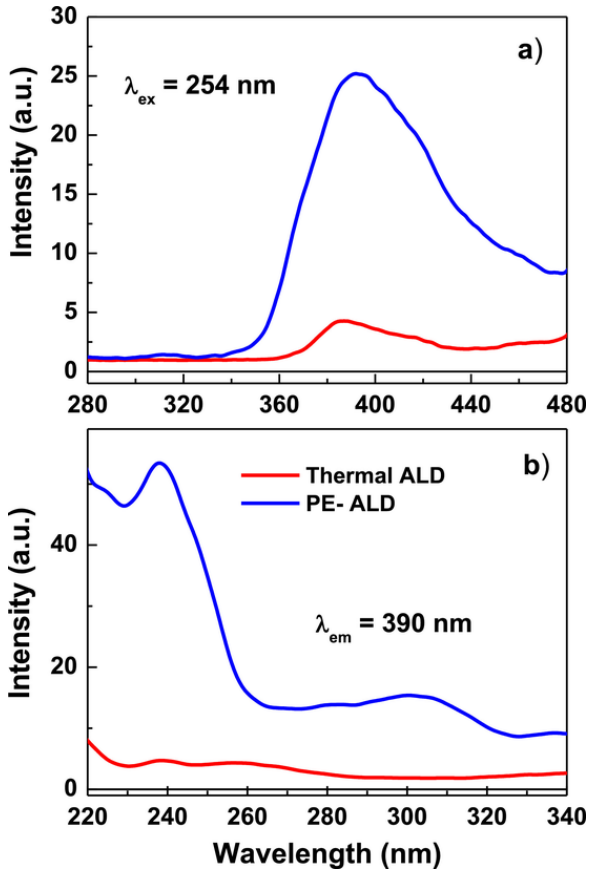

Fig. 6. Photoluminescence emission (a) and excitation (b) spectra of ALD and PE-ALD thin ZnO films.

3.3. Photocatalytic activity

Data obtained from measurements of the photodegradation of the MB dye in aqueous solution under UV illumination is shown in Fig. 7 a). To quantify the rate of degradation, we describe the concentration decay with one rate constant k [43]:

$$C(t) = C(0)\,exp(-kt)$$

where $C(0)$ is the initial dye concentration and t is the exposure time to UV illumination. Plotting the same data on the semi-logarithmic graph (Fig. 7 b), the rate constant k can be extracted from the slope of the straight portion of the plot:

$$ln\left[C(t)/C(0)\right] = -kt$$

The value for the rate constant for the ALD film, k_{ALD} = 0.8 × 10^{-3} min^{-1}, is comparable to values previously obtained by others [22, 38]. However, the rate constant for the PE-ALD film, k_{PEALD} = 2.7 × 10^{-3} min^{-1} cm^{-2} is even higher than the values for the most effective ALD films synthesised by thermal ALD at higher temperatures (> 150 °C). Apparently, we can achieve high photocatalytic activity of thin ZnO films even at low deposition temperatures by using the PE-ALD method.

It is known that ultrathin ZnO films deposited by thermal ALD lose their photocatalytic ability upon prolonged exposure to UV light in aqueous solution due to corrosion [44]. To test the stability of our PE-ALD ZnO thin films, we have performed several successive 7 hour degradation cycles on the same sample (see Supplementary Material). It is found that only after the 3rd cycle the photocatalytic activity of the film starts to deteriorate significantly. The equivalent set of measurements on thermal ALD samples shows a slight improvement in the photocatalytic activity, although it remains much lower compared to the photocatalytic activity of the PE-ALD film. Higher stability of the thin ZnO films used in our experiments compared to the films presented in [44] can be attributed to the higher thickness of our films (100 nm compared to 28 nm in [44]).

The photocatalytic activity of the ZnO film surface depends on a steady-state concentration of photoexcited charge carriers at the very surface. The steady-state concentration is determined by a rate of photogeneration and a rate of recombination. From the excitation spectra (Fig. 6 b), it can be seen that UV excitation is much more efficient in the PE-ALD film. Moreover, our measurements, as well as some previously published by other groups [24-26], have shown that the specific resistivity of the PE-ALD thin ZnO films, ρ > 10^4 Ωcm, is orders of magnitude higher than the resistivity of the thermally grown ALD thin ZnO films (typically ρ ~ 10 Ωcm for the films thermally grown at 100 °C). A lower degree of crystallinity of the PE-ALD also strongly reduces the charge carrier mobility and accordingly increases the charge carrier separation time, leading to a reduced recombination rate. Both effects lead to a higher charge concentration on the active semiconductor surface and thus to an increase in catalytic activity. It should be noted that these findings are in agreement with some previous research on nanostructured ZnO [45], where was also observed that a higher defect concentration promotes the photocatalytic activity of the ZnO material.

4. Conclusions

The results presented in this study reveal different morphology and texture properties of thin ZnO films synthesised by the PE-ALD method compared to the films synthesised by the thermal ALD method. Conse-

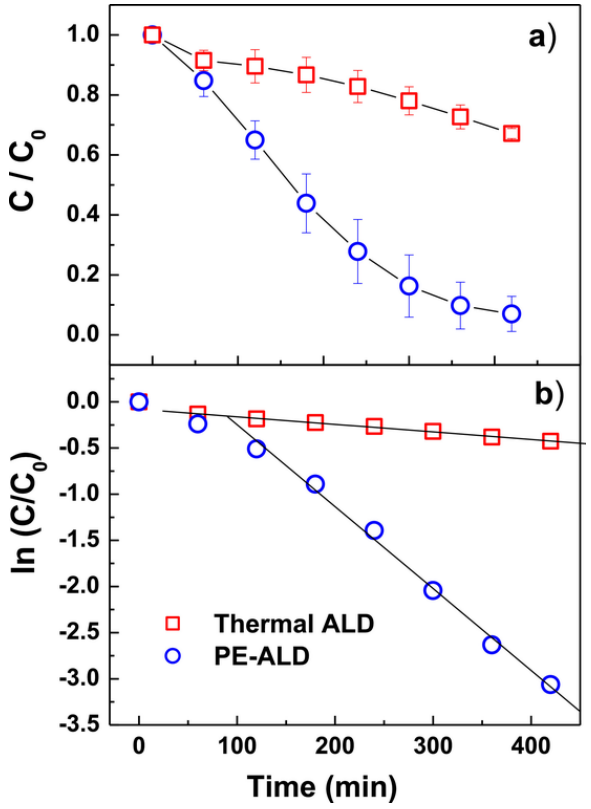

Fig. 7. Photodegradation curves of methylene blue dye in aqueous solution under UV illumination plotted in linear (a) and semi-logarithmic (b) plot.

quently, the PE-ALD films show different physical properties: much lower charge mobility and much higher excitation capacity in the UV spectral region. Such altered physical properties (compared to those of the thermally ALD synthesised thin ZnO films) lead to a strong, tenfold increase in photocatalytic activity.

CrediT

Ales Omerzu: Conceptualization, Photocatalysis and optical measurements, Data analysis, Writing – original draft, Funding
Robert Peter: ALD synthesis, XPS and SIMS measurements
Daria Jardas: ALD synthesis, Photocatalysis, SEM imaging
Iztok Turel: Optical spectroscopy, Photocatalysis, Writing – editing, Funding
Kresimir Salamon: XRD measurements and analysis
Matejka Podlogar: TEM sample preparation, SEM imaging
Damjan Vengust: HRTEM imaging and analysis
Ivana Jelovica Badovinac: EDX analysis
Ivna Kavre Piltaver: Initial SEM imaging
Mladen Petravic: Writing – review and editing, Funding

Declaration of Competing Interest

The authors declare no conflict of interest.

Acknowledgements

This work was supported in part by the Croatian Science Foundation (under project IP-2016-06-3568), the European Fund for Regional Development and the Ministry of Science, Education and Sports of the Republic of Croatia (under grant number RC.2.2.06-0001) and the University of Rijeka under projects numbers 18-144 and 18.13.2.1.01. It was also partly funded by Slovene Human Resources Development and Scholarship Fund as well as by European Fund for Regional Development (project number 217. JR) and the Slovenian Research Agency (grant number P1-0175). The authors would like to acknowledge Tina Radosevic for her invaluable help in sample preparation for HRTEM analysis.

Supplementary materials

Supplementary material associated with this article can be found, in the online version, at doi:10.1016/j.surfin.2021.100984.

References

[1] C. Jagadish, S. Pearton (Eds.), Zinc Oxide Bulk, Thin Films and Nanostructures: Processing, Properties, and Applications, Elsevier, Amsterdam, 2006.
[2] Ü. Özgür, D. Hofstetter, H. Morkoç, ZnO Devices and Applications: A review of Current Status and Future Prospects, Proc. IEEE 98 (2010) 1255–1268 htttps://doi.org/10.1109/JPROC.2010.2040363.
[3] M.C. Markham, K.J. Laidler, A Kinetic Study of Photo-oxidations on the Surface of Zinc Oxide in Aqueous Suspensions, J. Phys. Chem. 57 (1953) 363–369, https://doi.org/10.1021/j150504a027.
[4] T.R. Rubin, J.G. Calvert, G.T. Rankin, W. MacNevin, Photochemical Synthesis of Hydrogen Peroxide at Zinc Oxide Surfaces, J. Am. Chem. Soc. 75 (1953) 2850–2853, https://doi.org/10.1021/ja01108a017.
[5] S.R. Morrison, T. Freund, Chemical Role of Holes and Electrons in ZnO Photocatalysis, J. Chem. Phys. 47 (1967) 1543–1550, https://doi.org/10.1063/1.1712115.
[6] A. Sharma, P. Rao, R.P. Mathur, S.C. Ameta, Photocatalytic reactions of xylidine ponceau on semiconducting zinc oxide powder, J. Photochem. Photobiol. A 86 (1995) 197–200, https://doi.org/10.1016/1010-6030(94)03933-L.
[7] L. Selva Roselin, G.R. Rajarajeswari, R. Selvin, V. Sadasivam, B. Sivasankar, K. Rengaraj, Sunlight/ZnO-mediated photocatalytic degradation of reactive red 22 using thin film flat bed flow photoreactors, Solar Energy 73 (2002) 281–285, https://doi.org/10.1016/S0038-092X(02)00065-8.
[8] S. Mandal, R.K. Singha, A. Dhar, S.K. Ray, Optical and structural characteristics of ZnO thin films grown by rf magnetron sputtering, Mater. Res. Bull. 43 (2008) 244–250, https://doi.org/10.1016/j.materresbull.2007.05.006.
[9] F. Quaranta, A. Valentini, F.R. Rizzi, G. Casamassima, Dual-ion-beam sputter deposition of ZnO films, J. Appl. Phys. 74 (1993) 244–248, https://doi.org/10.1063/1.354152.
[10] Y. Chen, D.M. Bagnall, Z. Zhu, T. Sekiuchi, K. Park, K. Hiraga, T. Yao, S. Koyama, M.Y. Shen, T. Goto, Growth of ZnO single crystal thin films on c-plane (0 0 0 1) sapphire by plasma enhanced molecular beam epitaxy, J. Cryst. Growth 181 (1997) 165–169, https://doi.org/10.1016/S0022-0248(97)00286-8.
[11] Y. Chen, D.M. Bagnall, H. Koh, K. Park, K. Hiraga, Z. Zhu, T. Yao, Plasma assisted molecular beam epitaxy of ZnO on *c*-plane sapphire: Growth and characterization, J. Appl. Phys. 84 (1998) 3912–3918, https://doi.org/10.1063/1.368595.
[12] H. Liu, L. Feng, J. Zhai, L. Jiang, D.B. Zhu, Reversible Wettability of a Chemical Vapor Deposition Prepared ZnO Film between Superhydrophobicity and Superhydrophilicity, Langmuir 20 (2004) 5659–5661, https://doi.org/10.1021/la036280o.
[13] M. Purica, E. Budianu, E. Rusu, M. Danila, R. Gavrila, Optical and structural investigation of ZnO thin films prepared by chemical vapor deposition (CVD), Thin Solid Films 403 (2002) 485–488, https://doi.org/10.1016/S0040-6090(01)01544-9.
[14] T. Tynell, M. Karppinen, Atomic layer deposition of ZnO: a review, Semicond. Sci. Technol. 29 (15pp) (2014) 043001, https://doi.org/10.1088/0268-1242/29/4/043001.
[15] E.M. Kaidashev, M. Lorenz, H. von Wenckstern, A. Rahm, H.-C. Semmelhack, K.-H. Han, G. Benndorf, C. Bundesmann, H. Hochmuth, M. Grundmann, High electron mobility of epitaxial ZnO thin films on *c*-plane sapphire grown by multistep pulsed-laser deposition, Appl. Phys. Lett. 82 (2003) 3901–3903, https://doi.org/10.1063/1.1578694.
[16] R. Serhane, S. Abdelli-Messaci, S. Lafane, H. Khales, W. Aouimeur, A. Hassein-Bey, T. Boutkedjirt, Pulsed laser deposition of piezoelectric ZnO thin films for bulk acoustic wave devices, Appl. Surf. Sci. 288 (2014) 572–578, https://doi.org/10.1016/j.apsusc.2013.10.075.
[17] S. Mehla, J. Das, D. Jampaiah, S. Periasamy, A. Nafady, S.K. Bhargava, Recent advances in preparation methods for catalytic thin films and coatings, Catal. Sci. Technol. 9 (2019) 3582–3602, https://doi.org/10.1039/C9CY00518H.
[18] S. Sampath, M. Shestakova, P. Maydannik, T. Ivanova, T. Homola, A. Bryukvin, M. Sillanpää, R. Nagumothu, V. Alagan, Photoelectrocatalytic activity of ZnO coated nano-porous silicon by atomic layer deposition, RSC Adv 6 (2016) 25173–25178, https://doi.org/10.1039/C6RA01655C.
[19] B.-H. Mao, E. Crumlin, E.C. Tyo, M.J. Pellin, S. Vajda, Y. Li, S.-D. Wang, Z. Liu, In situ study of the electronic structure of atomic layer deposited oxide

ultrathin films upon oxygen adsorption using ambient pressure XPS, Catal. Sci. Technol. 6 (2016) 6778–6783, https://doi.org/10.1039/C6CY00575F.
[20] E. Guziewicz, I.A. Kowalik, M. Godlewski, K. Kopalko, V. Osinniy, A. Wójcik, S. Yatsunenko, E. Łusakowska, W. Paszkowicz, M. Guziewicz, Extremely low temperature growth of ZnO by atomic layer deposition, J. Appl. Phys. 103 (2008) 5 pp 033515, https://doi.org/10.1063/1.2836819.
[21] A. di Mauro, M. Cantarella, G. Nicotra, V. Privitera, G. Impellizzeri, Low temperature atomic layer deposition of ZnO: Applications in photocatalysis, Appl. Catal. B 196 (2016) 69–76 http://doi.org/10.1016/j.apcatb.2016.05.015.
[22] V. Rogé, N. Bahlawane, G. Lamblin, I. Fechete, F. Garin, A. Dinia, D. Lenoble, Improvement of the photocatalytic degradation property of atomic layer deposited ZnO thin films: the interplay between film properties and functional performances, J. Mater. Chem. A 3 (2015) 11453–11461, https://doi.org/10.1039/C5TA01637A.
[23] H.B. Profijt, S.E. Potts, M.C.M. van de Sanden, W.M.M. Kessels, Plasma-Assisted Atomic Layer Deposition: Basics, Opportunities, and Challenges, J. Vac. Sci. Technol. A 29 (2011) 25 pp 050801, https://doi.org/10.1116/1.3609974.
[24] S.-H.K. Park, C.-S. Hwang, H.-S. Kwack, J.-H. Lee, H.Y. Chu, Characteristics of ZnO Thin Films by Means of Plasma-Enhanced Atomic Layer Deposition, Electrochem. Solid-State Lett 9 (2006) G299–G301, https://doi.org/10.1149/1.2221770.
[25] D. Kim, H. Kang, J.M. Kim, H. Kim, The properties of plasma-enhanced atomic layer deposition (ALD) ZnO thin films and comparison with thermal ALD, Appl. Surf. Sci. 257 (2011) 3776–3779, https://doi.org/10.1016/j.apsusc.2010.11.138.
[26] M.A. Thomas, J.B. Cui, Highly Tunable Electrical Properties in Undoped ZnO Grown by Plasma Enhanced Thermal-Atomic Layer Deposition, Appl. Mater. Interfaces 4 (2012) 3122–3128, https://doi.org/10.1021/am300458q.
[27] J. Zhang, H. Yang, Q. Zhang, S. Dong, J.K. Luo, Structural, optical, electrical and resistive switching properties of ZnO thin films deposited by thermal and plasma-enhanced atomic layer deposition, Appl. Surf. Sci. 282 (2013) 390–395, https://doi.org/10.1016/j.apsusc.2013.05.141.
[28] M. Napari, M. Lahtinen, A. Veselov, J. Julin, E. Østreng, T. Sajavaara, Room-temperature plasma-enhanced atomic layer deposition of ZnO: Film growth dependence on the PEALD reactor configuration, Surf. Coat. Tech. 326 (2017) 281–290, https://doi.org/10.1016/j.surfcoat.2017.07.056.
[29] J. Pilz, A. Perrotta, P. Christian, M. Tazreiter, R. Resel, G. Leising, T. Griesser, A.M. Coclite, Tuning of material properties of ZnO thin films grown by plasma-enhanced atomic layer deposition at room temperature, J. Vac. Sci. Tech. A 36 (2018) 01A109 9 pp, https://doi.org/10.1116/1.5003334.
[30] Y. Zheng, C. Chen, Y. Zhan, X. Lin, Q. Zheng, K. Wei, J. Zhu, Y. Zhu, Luminescence and Photocatalytic Activity of ZnO Nanocrystals: Correlation between Structure and Property, Inorg. Chem. 46 (2007) 6675–6682, https://doi.org/10.1021/ic062394m.
[31] Q. Wang, Y. Li, Z. Zeng, S. Pang, Relationship between crystal structure and luminescent properties of novel red emissive $BiVO_4$:Eu^{3+} and its photocatalytic performance, J. Nanopart. Res. 14 (2012) 1076, https://doi.org/10.1007/s11051-012-1076-1T.
[32] D. Lu, Y. Tang, J. Gao, Q. Wang, Concentrated solar irradiation protocols for the efficient synthesis of tri-color emissive carbon dots and photophysical studies, J. Mat. Chem. C 6 (2018) 13013–13022 E.
[33] J. Végh, The Shirley background revised, J. Electron Spetrosc. 151 (2006) 159–164, https://doi.org/10.1016/j.elspec.2005.12.002.
[34] M. Podlogar, J.J. Richardson, D. Vengust, N. Daneu, Z. Samardzija, S. Bernik, A. Recnik, Growth of transparent and conductive polycrystalline (0001)-ZnO films on glass substrates under low-temperature hydrothermal conditions, Adv. Funct. Mater. 22 (2012) 3136–3145, https://doi.org/10.1002/adfm.201200214.
[35] D. Meljanac, K. Juraić, M. Plodinec, Z. Siketić, D. Gracin, N. Krstulović, K. Salamon, H. Skenderović, Z. Kregar, I. Šrut Rakić, S. Bernstorff, Influence of RF excitation during pulsed laser deposition in oxygen atmosphere on the structural properties and luminescence of nano-crystalline ZnO:Al thin films, J. Vac. Sci. Technol. A 34 (2016) 10 pp 021514, https://doi.org/10.1116/1.4941197.
[36] K. Salamon, O. Milat, N. Radić, P. Dubček, M. Jerčinović, S. Bernstorff, Structure and morphology of magnetron sputtered W films studied by x-ray methods, J. Phys. D: Appl. Phys. 46 (10pp) (2013) 095304, https://doi.org/10.1088/0022-3727/46/9/095304.
[37] M.C. Biesinger, B.P. Payne, A.P. Grosvenor, L.W.M. Lau, A.R. Gerson, R.S.C. Smart, Resolving surface chemical states in XPS analysis of first row transition metals, oxides and hydroxides: Cr, Mn, Fe, Co and Ni, Appl. Surf. Sci. 257 (2011) 2717–2730, https://doi.org/10.1016/j.apsusc.2010.10.051.
[38] R. Peter, K. Salamon, A. Omerzu, J. Grenzer, I. Jelovica Badovinac, I. Saric, M. Petravic, Role of Hydrogen-Related Defects in Photocatalytic Activity of ZnO Films Grown by Atomic Layer Deposition, J. Phys. Chem. C 124 (2020) 8861–8868, https://doi.org/10.1021/acs.jpcc.0c01519.
[39] J.-C. Dupin, D. Gonbeau, P. Vinatier, A. Levasseur, Systematic XPS studies of metal oxides, hydroxides and peroxides, Phys. Chem. Chem. Phys. 2 (2000) 1319–1324, https://doi.org/10.1039/A908800H.
[40] M. Krzywiecki, L. Grządziel, A. Sarfraz, D. Iqbal, A. Szwajca, A. Erbe, Zinc oxide as a defect-dominated material in thin films for photovoltaic applications – experimental determination of defect levels, quantification of composition, and construction of band diagram, Phys. Chem. Chem. Phys. 17 (2015) 10004–10013, https://doi.org/10.1039/C5CP00112A.
[41] E. Guziewicz, M. Godlewski, L. Wachnicki, T.A. Krajewski, G. Luka, S. Gieraltowska, R. Jakiela, A. Stonert, W. Lisowski, M. Krawczyk, J.W. Sobczak, A. Jablonski, ALD grown zinc oxide with controllable electrical properties, Semicond. Sci. Technol. 27 (11pp) (2012) 074011, https://doi.org/10.1088/0268-1242/27/7/074011.
[42] R. Hong, H. Qi, J. Huang, H. He, Z. Fan, J. Shao, Influence of oxygen partial pressure on the structure and photoluminescence of direct current reactive magnetron sputtering ZnO thin films, Thin Solid Films 473 (2005) 58–62, https://doi.org/10.1016/j.tsf.2004.06.159.
[43] M.A. Behnajady, N. Modirshahla, R. Hamzavi, Kinetic study on photocatalytic degradation of C.I. Acid Yellow 23 by ZnO photocatalyst, J. Hazard. Mater. B 133 (2006) 226–232, https://doi.org/10.1016/j.jhazmat.2005.10.022.
[44] Y.-Q. Cao, J. Chen, H. Zhou, X. Li, Z.-Y. Cao, D. Wu, A.-D. Li, Photocatalytic activity and photocorrosion of atomic layer deposited ZnO ultrathin films for the degradation of methylene blue, Nanotecnology 26 (2015) 024002, https://doi.org/10.1088/0957-4484/26/2/024002.
[45] J. Gupta, K.C. Barick, D. Bahadur, Defect mediated photocatalytic activity in shape-controlled ZnO nanostructures, J. Alloy Compd. 509 (2011) 6725–6730, https://doi.org/10.1016/j.jallcom.2011.03.157.